





Goos-Hänchen shifts in a combined tripod and Λ atom-light coupling scheme

Muqaddar Abbas ^{1,*}, Seyyed Hossein Asadpour ^{2,†}, Ziauddin ³, Pei Zhang ^{1,‡}, Julius Ruseckas ⁴,
and Hamid R. Hamed ^{5,§}

¹Ministry of Education Key Laboratory for Nonequilibrium Synthesis and Modulation of Condensed Matter, Shaanxi Province Key Laboratory of Quantum Information and Quantum Optoelectronic Devices, School of Physics, Xi'an Jiaotong University, Xi'an 710049, China

²School of Physics, Institute for Research in Fundamental Sciences (IPM), Tehran 19395-5531, Iran

³Quantum Optics Lab. Department of Physics, COMSATS University Islamabad, Islamabad 45550, Pakistan

⁴Baltic Institute of Advanced Technology, Pilies St. 16-8, LT-01403 Vilnius, Lithuania

⁵Institute of Theoretical Physics and Astronomy, Vilnius University, Sauletekio 3, Vilnius 10257, Lithuania



(Received 8 November 2023; revised 20 May 2024; accepted 12 August 2024; published 27 August 2024)

We investigate the controlled manipulation of the Goos-Hänchen (GH) shift in probe light beams, encompassing both plane and Gaussian beams, when introduced into a cavity housing a highly resonant five-level atomic system exhibiting a combined tripod and Λ (CTL) configuration. This complex scheme arises from the interaction of three atomic ground states with two excited states through five distinct light fields. Such a system effectively reduces to a Λ - or N-shaped configuration by manipulating the light fields, resulting in the alteration of the dispersion behavior of the probe beam, ultimately inducing either a positive or negative GH shift. This unique behavior is a direct consequence of the closed-loop structure inherent to the five-level atomic scheme. For both plane and Gaussian beams, we demonstrate the superiority of CTL over Λ and N schemes in achieving substantial positive GH shifts. When considering Gaussian probe light, we observe a critical role played by the beam width in controlling the magnitude and sign of the GH shifts. Our proposed approach for studying the GH shift carries significant practical implications, particularly in its capacity to monitor media with either left-handed characteristics displaying negative permittivity and permeability or right-handed characteristics displaying positive permittivity and permeability through the manipulation of externally controlled parameters. This approach may find applications in various fields, including optical heterodyne sensors used to measure beam angle, displacement, temperature, and refractive index, thereby advancing our understanding and control of optical phenomena.

DOI: [10.1103/PhysRevA.110.023730](https://doi.org/10.1103/PhysRevA.110.023730)

I. INTRODUCTION

The Goos-Hänchen (GH) shift is a phenomenon characterized by the lateral displacement of incident and reflected light beams at the interface of two media, especially when the incidence angle exceeds the critical angle. Its wide range of applications spans various fields, including nonlinear optics [1], quantum mechanics [2,3], micro and nanooptics [4], optical sensors [5], plasma physics [6], neutron physics [7], and acoustics [8].

The GH shift arises due to the angular dispersion of the phase delay of light beams. This intriguing effect can be deliberately induced by manipulating the phase delay, as documented in numerous material systems and structures. Noteworthy examples include graphene [9,10], photonic crystals [11], metals [12,13], and absorbing media [14].

The first experimental investigation of the GH shift was carried out by Goos and Hänchen in 1947 [15]. They employed multiple reflections within a glass slab to study transverse electric (TE) polarized light beams. In 1948,

Artmann proposed this effect by incorporating the stationary phase theory [16]. It's worth noting that Artmann's analytical findings extended to transverse magnetic (TM) polarized light beams. In 1949, Goos and Hänchen experimentally confirmed these results for TM polarized light beams [17].

In 1964, Renard introduced an alternative theoretical approach for studying the GH shift based on the energy flux technique [18]. The first observation of a spectral resonance in the lateral displacement of a laser beam totally reflected from a glass-cesium vapor interface was reported in Ref. [19]. Shift and broadening in attenuated total reflection spectra of the hyperfine-structure-resolved D_2 line of dense rubidium vapor was observed in Ref. [20]. The theoretical predictions of the GH shift were later experimentally validated [21].

Observing the GH shift experimentally can be challenging due to its small amplitude, typically on the order of a few wavelengths. To overcome this, researchers have explored various frameworks and materials to enhance the GH shift's amplitude, as outlined in Ref. [22]. One approach to achieve an enhanced positive GH shift is by incorporating multilayered periodic structures [23] and waveguide structures [24,25]. Conversely, an enhanced negative GH shift can be achieved through the use of a slab design with a dielectric medium possessing maximum absorption capacity, as well as metamaterials [26].

*Contact author: muqaddarabbas@xjtu.edu.cn

†Contact author: asadpour@ipm.ir

‡Contact author: zhangpei@mail.ustc.edu.cn

§Contact author: hamid.hamed@tfai.vu.lt

It is important to note that the GH shift exhibits polarization state dependence. Specifically, this information is relevant for both TM and TE polarized light. Under the same conditions, the reflection coefficients for these two polarizations differ, leading to variations in the GH shift, as discussed in Refs. [13,26].

The modulation, as opposed to amplification, of the GH-shift magnitude plays a pivotal role in this context. This procedure involves an investigation of an atomic medium, a quantum dot, and a quantum well, all situated within a cavity. The objective is then to determine the extent of the GH shift by manipulating externally provided control parameters. Coherent control fields can influence the absorption and dispersion responses of the medium within the cavity [27–37]. Notably, it has been observed that increased GH shift occurs at the point of darkness in an asymmetric Fabry-Perot cavity consisting of four layers when oriented at the Brewster angle [38]. Similarly, a cavity featuring an atomic medium with a double ladder-type atomic configuration was employed to generate adjustable positive and negative GH shift. Theoretical investigations have also explored the effects of broadband squeezed vacuum fields on GH shifts in reflected and transmitted light beams, with control parameters including photon number and phase difference relative to the control field, as indicated in Ref. [5]. Furthermore, enhanced GH shift has been experimentally achieved by exciting surface plasmons (SPs) on a metal surface, as described in Ref. [39]. The excited surface waves lead to a narrow resonance in the angular reflectance spectrum. Theoretical studies have delved into the GH shift in the context of a long-range surface plasmon setup, revealing the involvement of orders of magnitude greater than the wavelength [40,41]. A recent study observed giant GH and angular shifts at designed metasurfaces [42].

In contrast, slabs characterized by spatially inhomogeneous permittivity, dependent on the intensity of incident light, harnessed their GH shifts in a different manner when examining reflection, as explored in Ref. [43]. Both theoretical and experimental investigations aimed to understand the distinct behaviors of edge reflection in two-dimensional graphene plasmons. In the presence of evanescent waves, these plasmons gave rise to negative GH shift, with the unexpected amplitude oscillation of odd-even peaks attributed to wave diffraction near the edge, as demonstrated in Ref. [44]. Additionally, the GH shift associated with pseudospin-3/2 Dirac-Weyl fermions was explored in the context of birefringence [45]. A graphene plasmonic metasurface was employed to examine the potential for substantial and controllable GH shift in the center of gravity of the reflected light beam [46].

The GH shift holds significant potential for various applications in optical heterodyne devices. It serves as a valuable tool for monitoring parameters such as temperature, beam angle, displacement, and refractive index. Furthermore, it provides insights into material characteristics based on permittivity and permeability, distinguishing between left-handed (negative permittivity and permeability) and right-handed (positive permittivity and permeability) materials. The GH shift can also be employed to detect irregularities, surface roughness, and other features on isotropic materials that are uniformly distributed in space. Its adaptability allows for

versatile applications, making it a powerful tool for optical switches and sensors. To achieve this adaptability, various methods have been proposed to alter the GH shift by adjusting temperature, electric fields, and light fields [28]. Furthermore, research has delved into the plasmon-induced transparency region surrounding a tunable GH shift in a metal-insulator-metal structure, as investigated in Ref. [47]. Theoretical evidence supports the generation of significant GH shifts through surface modes at parity-time symmetric interfaces at specific incidence angles, as reported in Ref. [48]. The GH shift in both the reflected and transmitted beams can be enhanced by coupling to a broadband-squeezed vacuum field within a cavity that features a two-level atom as the intracavity medium, as discussed in Ref. [5]. Notably, the relative phase between the compressed vacuum field and the control field applied to the two-level atom has a substantial impact on the GH shift in both scenarios. The GH shift was also calculated for resonance and nonresonance states of plane waves, with consideration of atomic-cavity coupling [49]. In these circumstances, a considerable GH shift, whether positive or negative, was observed for both the transmitted and reflected light beams, emphasizing the potential and versatility of this phenomenon.

Recently, a novel atom-light coupling scheme, known as the combined tripod and Λ (CTL) scheme, was introduced for electromagnetically induced transparency (EIT) and slow light [50,51]. This scheme involved three atomic ground states interacting with two excited states through five light fields. Notably, it enabled the formation of dark states, a crucial element in achieving EIT and slow light. In the limiting cases, this scheme reduced to conventional Λ - or N -type atom-light couplings, providing EIT (with subluminality) or absorption (with superluminality), respectively.

In the context of this paper, we aim to investigate the tunability of the GH shift in the CTL model using a plane probe light beam [27,49] and a Gaussian beam [30,32]. The key motivation for this study arises from the significant advantages of the CTL scheme compared to its two limiting cases: the Λ and N -type atomic systems. The CTL scheme results in a more substantial positive GH -shift in the reflected beam when compared to the three-level Λ scheme. Additionally, it offers the capability for precise control and enhancement of GH shifts by manipulating the intensities of four control fields and their relative phases. Such a level of control is absent in the basic Λ scheme [34].

In contrast to the N -type system, the CTL model can generate a positive GH shift in the reflected beam, while the N -type system typically leads to negative shifts due to its inherent strong absorption and superluminal effects [35]. The CTL system introduces an innovative approach to EIT and slow light, resulting in prominent positive GH shifts in the reflected beam, as demonstrated in this study. These compelling advantages provide the foundation for our investigation into GH-shift properties within the CTL scheme.

We begin by examining a plane probe light beam and analyzing the reflection coefficient. Our goal is to explore the possibilities of achieving both positive and negative GH shifts in the reflected probe light beam by varying externally provided control parameters, which cause the intracavity medium to behave as Λ , N , and CTL systems. Furthermore,

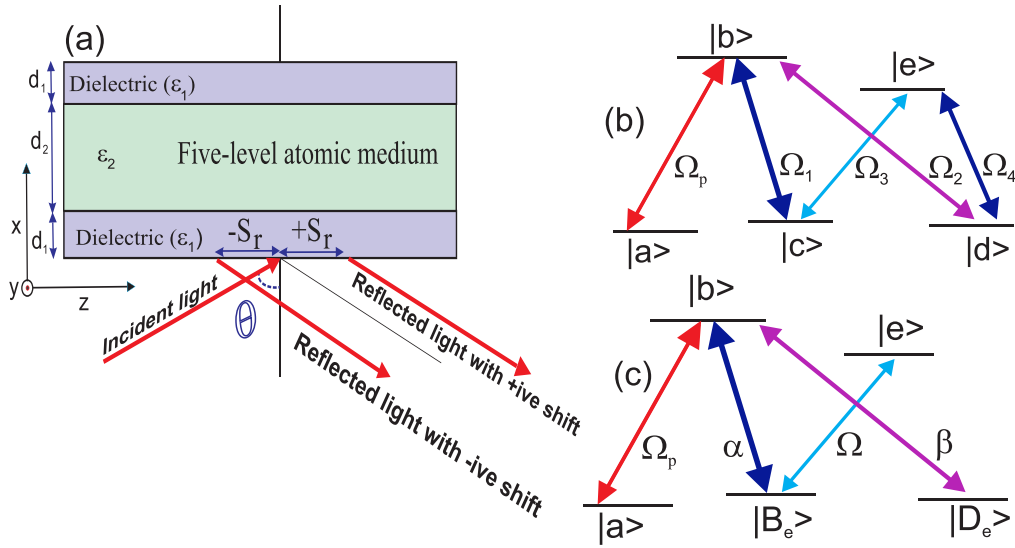


FIG. 1. (a) Schematic diagram of three layers cavity; the walls of cavity have thickness d_1 and fixed permittivity ϵ_1 and the intracavity medium contains five-level atomic medium having thickness d_2 and permittivity ϵ_2 . Also negative and positive GH shift are denoted by $-S_r$ and $+S_r$, (b) Five-level combined tripod and Λ atomic system, (c) Five-level combined tripod and Λ atomic system in the transformed basis for $\alpha, \beta \neq 0$.

we consider the Gaussian probe light beam and assess the impact of beam width. The width of the Gaussian beam plays a crucial role in determining the GH shift. A narrow Gaussian beam width results in a wide spectrum and a sharp profile because it penetrates more deeply into the medium, leading to a larger GH shift. Conversely, an increase in Gaussian beam width reduces the GH shift, and the shift remains nearly constant for very large values of the Gaussian beam width. This is due to the fact that, for a large Gaussian beam width, the characteristics of the Gaussian light resemble those of a uniform plane wave.

II. THEORETICAL FRAMEWORK

Let us consider a TE-polarized probe light beam denoted as E_p , which impinges on a three-layer cavity from vacuum with ($\epsilon_0 = 1$), as illustrated in Fig. 1(a). The cavity walls are constructed from two dielectric materials characterized by fixed permittivity ϵ_1 and thickness d_1 . The intracavity medium's permittivity, denoted as ϵ_2 , is associated with the dielectric susceptibility of the CTL atomic medium and has a thickness of d_2 .

The CTL model involves a complex intercoupling, featuring a four-level tripod subsystem that includes the ground states $|a\rangle$, $|c\rangle$, $|d\rangle$, and the excited state $|b\rangle$. Additionally, there is a three-level Λ subsystem comprising the ground states $|c\rangle$, $|d\rangle$, and the excited state $|e\rangle$. These subsystems are interconnected through the influence of a probe field and four control laser fields, as depicted in Fig. 1(b).

The interaction is facilitated by four control laser fields characterized by Rabi frequencies Ω_1 , Ω_2 , Ω_3 , and Ω_4 . These fields establish connections between the excited states $|b\rangle$ and $|e\rangle$ through two distinct pathways: $|b\rangle \rightarrow |c\rangle \rightarrow |e\rangle$ and $|b\rangle \rightarrow |d\rangle \rightarrow |e\rangle$. This configuration results in the creation of a four-level closed-loop coherent coupling scheme, which can

be described by the Hamiltonian

$$H_{4\text{Levels}} = -\Omega_1^*|c\rangle\langle b| - \Omega_2^*|d\rangle\langle b| - \Omega_3^*|c\rangle\langle e| - \Omega_4^*|d\rangle\langle e| + \text{H.c.} \quad (1)$$

A weak probe field described by a Rabi frequency Ω_p couples then the closed-loop subsystem to a ground level $|a\rangle$ via the atomic transition $|a\rangle \leftrightarrow |b\rangle$. The destructive interference between different transition pathways induced by the control and probe beams can make the medium transparent for the resonant probe beam in a narrow frequency range due to the EIT [50,51]. The total Hamiltonian of the system involving all five atomic levels of the CTL level scheme is then described by

$$H_{5\text{Levels}} = -(\Omega_p^*|a\rangle\langle b| + \Omega_p|b\rangle\langle a|) + H_{4\text{Levels}}. \quad (2)$$

In Fig. 1(c), we illustrate the five-level CTL atomic system in a transformed basis. Switching to a new basis, the Hamiltonian describing the four-level atomic subsystem featured in Eq. (1) can be represented as

$$H_{4\text{Levels}} = -\beta|D_e\rangle\langle b| - \alpha|B_e\rangle\langle b| - \Omega|B_e\rangle\langle e| + \text{H.c.}, \quad (3)$$

where $|D_e\rangle = \frac{1}{\Omega}(\Omega_4|c\rangle - \Omega_3|d\rangle)$ and $|B_e\rangle = \frac{1}{\Omega}(\Omega_3^*|c\rangle + \Omega_4^*|d\rangle)$ are the internal dark and bright states for the Λ scheme composed of the two ground states $|c\rangle$ and $|d\rangle$, as well as an excited states $|e\rangle$. In writing Eq. (3), we define

$$\beta = \frac{1}{\Omega}(\Omega_1^*\Omega_4^* - \Omega_2^*\Omega_3^*), \quad (4)$$

$$\alpha = \frac{1}{\Omega}(\Omega_1^*\Omega_3^* + \Omega_2^*\Omega_4^*), \quad (5)$$

where we define the total Rabi frequency

$$\Omega = \sqrt{|\Omega_3|^2 + |\Omega_4|^2}. \quad (6)$$

By changing the Rabi frequencies of the control fields one can control the coefficients β and α arriving at three different situations: (i) both α and β are nonzero; (ii) β is zero; (iii) α is zero. When both α and β are nonzero ($\alpha, \beta \neq 0$), there exists a superposition state

$$|D\rangle = \beta|a\rangle - \Omega_p|D_e\rangle. \quad (7)$$

The superposition state $|D\rangle$ in Eq. (7) is composed of contributions from both the ground level $|a\rangle$ and the internal dark state $|D_e\rangle$ of the sub- Λ system, constructed from the bare states $|c\rangle$ and $|d\rangle$. It excludes any contribution from the excited states $|b\rangle$ and $|e\rangle$, establishing itself as a global dark state for the entire CTL system. In simpler terms, if the atom is initially in the state $|D\rangle$, there is no possibility of excitation to the excited states $|b\rangle$ and $|e\rangle$, preventing subsequent spontaneous emission.

In the case of a weak probe field ($\Omega_p \ll \Omega_1, \Omega_2, \Omega_3, \Omega_4$), it becomes evident that the dark state $|D\rangle$ effectively simplifies to $\beta|a\rangle$, precluding any possibility of excitation. This implies that the ground state $|a\rangle$ effectively becomes a dark state, rendering it unresponsive to incident light and creating a transparency window around the zero probe detuning Δ_p .

In the CTL scheme, the dynamics of the probe field and the atomic coherences can be described by the optical Bloch equations. When expressed in the new basis, the reduced

optical Bloch equations take on their specific form as

$$\begin{aligned} \dot{\rho}_{ba} &= -(\Gamma_b/2 - i\Delta_p)\rho_{ba} + i\alpha\rho_{B_ea} + i\beta\rho_{D_ea} \\ &\quad + i\Omega_p, \\ \dot{\rho}_{B_ea} &= i\Delta_p\rho_{B_ea} + i\alpha^*\rho_{ba} + i\Omega\rho_{ea}, \\ \dot{\rho}_{D_ea} &= i\Delta_p\rho_{D_ea} + i\beta^*\rho_{ba}, \\ \dot{\rho}_{ea} &= -(\Gamma_e/2 - i\Delta_p)\rho_{ea} + i\Omega\rho_{B_ea}. \end{aligned} \quad (8)$$

Here ρ_{ba} represents the optical coherence associated with the probe transition from $|a\rangle$ to $|b\rangle$, while ρ_{B_ea} , ρ_{D_ea} , and ρ_{ea} represent the ground-state coherences between $|a\rangle$ and $|B_e\rangle$, $|D_e\rangle$, or $|e\rangle$, respectively. As the probe field is assumed to be significantly weaker than the control fields, most of the atomic population resides in the ground state, allowing us to treat the probe field as a perturbation. All rapidly oscillating exponential factors associated with central frequencies and wave vectors are removed from the equations, leaving only the slowly varying amplitudes. We define the probe detuning as $\Delta_p = \omega_p - \omega_{ba}$, where ω_p represents the central frequency of the probe field. The control fields are assumed to be on resonance. Two excited states $|b\rangle$ and $|e\rangle$ decay with rates Γ_b and Γ_e , respectively.

From the coupled equations presented in (8), it is straightforward to derive the steady-state solution for the density matrix element ρ_{ba}

$$\rho_{ba} = \Omega_p \frac{\Delta_p(-|\Omega|^2 + i\Delta_p(\Gamma_e/2 - i\Delta_p))}{i\Delta_p(\Gamma_e/2 - i\Delta_p)\zeta + i|\Omega|^2\Delta_p(\Gamma_b/2 - i\Delta_p) + (\Gamma_b/2 - i\Delta_p)\Delta_p^2(\Gamma_e/2 - i\Delta_p) - |\Omega|^2|\beta|^2}, \quad (9)$$

where $\zeta = |\alpha|^2 + |\beta|^2$. The dielectric susceptibility is given by the relation

$$\chi = \eta\rho_{ba}, \quad (10)$$

where $\eta = N|\mu_{ba}|^2/(\epsilon_0\hbar)$, and

$$\epsilon_2 = 1 + \chi. \quad (11)$$

To investigate the behavior of the GH shift in the reflected beam for our system, we need to find the reflection coefficient of the field for the whole configuration. To this end, we rely on the approach of the transfer matrix [27,49] as we have the three-layer system. The transfer matrix for the j th layer of a given configuration is expressed as

$$N_j(k_z, \omega_p, d_j) = \begin{pmatrix} \cos[k_x^j d_j] & \frac{i\sin[k_x^j d_j]}{q_j} \\ iq_j \sin[k_x^j d_j] & \cos[k_x^j d_j] \end{pmatrix}. \quad (12)$$

Here, $k_x^j = \sqrt{\epsilon_j k^2 - k_z^2}$ is the x component of the wave vector in the j th layer of the medium, similarly the thickness of the j th layer is given by d_j , where j shows the number of the corresponding layer of the medium and $q_j = \frac{k_x^j}{k}$. Further k_z is the z component of wave vector in a vacuum. In our case, we have three layers; 1 and 3 are the cavity walls and 2 is the intracavity medium. The total transfer matrix for the incident and reflected probe light beam for our proposed model can be

written as [27]

$$x(k_z, \omega_p) = N_1(k_z, \omega_p, d_1)N_2(k_z, \omega_p, d_2)N_3(k_z, \omega_p, d_3). \quad (13)$$

Upon performing a series of mathematical derivations and calculations, the reflection coefficient can be determined as [27,49]

$$r(k_z, \omega_p) = \frac{q_o(x_{22} - x_{11}) - (q_o^2 x_{12} - x_{21})}{q_o(x_{22} + x_{11}) - (q_o^2 x_{12} + x_{21})}, \quad (14)$$

where x_{ij} are the elements of transfer matrix $x(k_z, \omega_p)$ and $q_o = \sqrt{\epsilon_o - \sin^2[\theta]}$.

III. STEADY-STATE ABSORPTION-DISPERSION CHARACTERISTICS

Figures 2(a) to 2(c) illustrates the absorption and dispersion characteristics of the scheme in three different scenarios: (i) when both α and β are nonzero (corresponding to a five-level CTL model); (ii) in the limiting case where β is zero (representing a four-level N -type model); and (iii) in the scenario where α is zero (characteristic of a three-level Λ model). For all simulations we consider $\Gamma_e = \Gamma$, $\Gamma_b = \Gamma$, $\eta = 0.01\Gamma$ and all parameters are scaled by Γ .

Due to the intricate and distinct nature of the three schemes arising from varying Rabi frequencies and relative phase requirements, it is imperative to adjust these parameters individually. Notably, it is not possible to use identical values

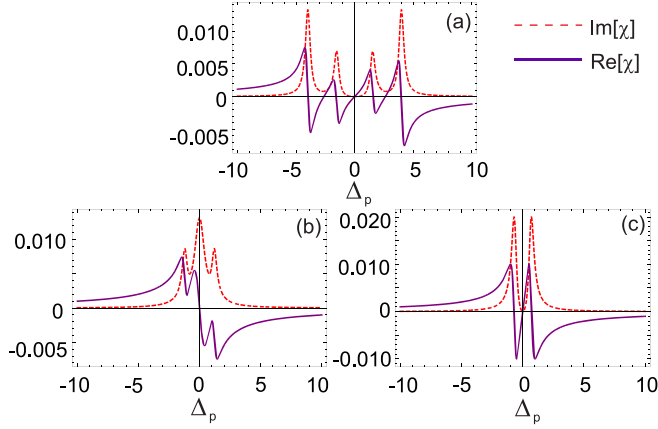


FIG. 2. The absorption (red dashed line) and dispersion behavior (purple solid line) of the five-level scheme for (a) $\Omega_1 = 1.5\Gamma$, $\Omega_2 = 3\Gamma$, $\Omega_3 = 2.5\Gamma$, $\Omega_4 = 0.9\Gamma$, and $\phi = 0$, satisfying $\alpha \neq 0$ and $\beta \neq 0$; (b) $\Omega_1 = 0.5\Gamma$, $\Omega_2 = 0.5\Gamma$, $\Omega_3 = 0.7\Gamma$, $\Omega_4 = 0.7\Gamma$, and $\phi = 0$, satisfying $\beta = 0$ and $\alpha \neq 0$; (c) $\Omega_1 = 0.5\Gamma$, $\Omega_2 = 0.5\Gamma$, $\Omega_3 = 0.7\Gamma$, $\Omega_4 = 0.7\Gamma$, and $\phi = \pi$, fulfilling $\alpha = 0$ but $\beta \neq 0$. In all simulations, we consider $\Gamma_e = \Gamma_b = \Gamma$.

of Rabi frequencies because they must be altered to achieve the different configurations. In the following and forthcoming sections concerning the analysis of GH shifts, we select parameters to accommodate each level scheme CTL, N , and Λ . Specifically, we set the following parameter values: $\Omega_1 = 1.5\Gamma$, $\Omega_2 = 3\Gamma$, $\Omega_3 = 2.5\Gamma$, $\Omega_4 = 0.9\Gamma$, and $\phi = 0$ to meet the conditions where $\alpha \neq 0$ and $\beta \neq 0$ (CTL model); $\Omega_1 = 0.5\Gamma$, $\Omega_2 = 0.5\Gamma$, $\Omega_3 = 0.7\Gamma$, $\Omega_4 = 0.7\Gamma$, and $\phi = 0$ to satisfy $\beta = 0$ and $\alpha \neq 0$ (N model); and $\Omega_1 = 0.5\Gamma$, $\Omega_2 = 0.5\Gamma$, $\Omega_3 = 0.7\Gamma$, $\Omega_4 = 0.7\Gamma$, and $\phi = \pi$ to fulfill $\alpha = 0$ but $\beta \neq 0$ (Λ scheme).

The results demonstrate the presence of slow light in cases (i) and (iii), where the positive slope of dispersion indicates a positive group index. In contrast, case (ii) exhibits superluminality, as evidenced by absorption with a negative slope of dispersion and, consequently, a negative group index. In the following section, we will explore the GH shifts for these three scenarios.

IV. CONTROL OVER GOOS-HÄNCHEN SHIFTS

A. GH shift for incident plane light beam

We initiate by examining an incident plane probe light beam directed at a three-layer cavity medium, making an angle θ with the normal. Utilizing the stationary phase theory, we can compute the GH shift in the reflected light for the incident plane probe light beam as

$$S_r = -\frac{\lambda_p}{2\pi} \frac{d\varphi_r}{d\theta}, \quad (15)$$

where λ_p is the wavelength of incident probe light beam and φ_r is the phase of the reflection coefficient.

The GH shift of the reflected light, as described in Eq. (15), can be reformulated in terms of the reflection coefficient r and

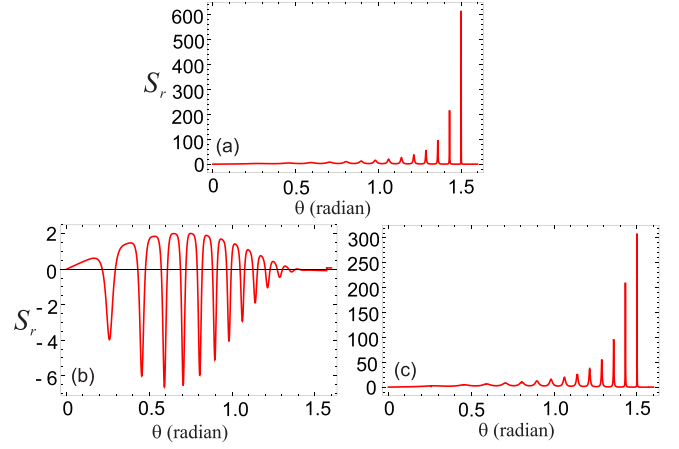


FIG. 3. The magnitude of GH shift (S_r) for plane beam versus angle of incidence (θ_p): (a) $\Omega_1 = 1.5\Gamma$, $\Omega_2 = 3\Gamma$, $\Omega_3 = 2.5\Gamma$, $\Omega_4 = 0.9\Gamma$, and $\phi = 0$ satisfying $\alpha \neq 0$ and $\beta \neq 0$; (b) $\Omega_1 = 0.5\Gamma$, $\Omega_2 = 0.5\Gamma$, $\Omega_3 = 0.7\Gamma$, $\Omega_4 = 0.7\Gamma$, and $\phi = 0$ satisfying $\beta = 0$ and $\alpha \neq 0$; (c) $\Omega_1 = 0.5\Gamma$, $\Omega_2 = 0.5\Gamma$, $\Omega_3 = 0.7\Gamma$, $\Omega_4 = 0.7\Gamma$, $\phi = \pi$, fulfilling $\alpha = 0$ but $\beta \neq 0$. The other parameters are $d_1 = 0.2\mu\text{m}$, $d_2 = 7.2\mu\text{m}$, $\epsilon_1 = 2.22$, $\epsilon_0 = 1$, $\Delta_p = 0.001\Gamma$ and $\Gamma_e = \Gamma_b = \Gamma$.

is represented as

$$S_r = -\frac{\lambda_p}{2\pi |r(k_z, \omega_p)|^2} \left\{ \text{Re}[r(k_z, \omega_p)] \frac{d\text{Im}[r(k_z, \omega_p)]}{d\theta} - \text{Im}[r(k_z, \omega_p)] \frac{d\text{Re}[r(k_z, \omega_p)]}{d\theta} \right\}. \quad (16)$$

As previously mentioned, the group index of the intracavity medium plays a pivotal role in shaping the behavior and magnitude of the reflected GH shift [28,32]. In the following, we will explore the GH shift of reflected light using Eq. (16), taking into account the intracavity medium in three distinct cases, where we vary α and β , thus resulting in our model behaving as a three, four, and five-level system. By considering these different intracavity scenarios, the group index of the medium undergoes variations, which directly impact the reflected GH shift.

1. Case 1: Both α and β are nonzero

We investigate the behavior of the GH shift in reflected light beams by examining a three-layer cavity in which the intracavity medium is sandwiched between two dielectric slabs. In this analysis, we consider an intracavity atomic medium with nonzero values for α and β which gives rise to the CTL system. The EIT and normal dispersion characteristics of the CTL system positioned between two dielectric slabs is illustrated in Fig. 2(a). The incident light originates from a vacuum medium with a dielectric constant of $\epsilon_0 = 1$ and strikes the cavity wall at an angle θ relative to the x axis. The resulting reflection of light may lead to a positive or negative GH-shift, depending on the overall group index of the medium.

In Fig. 3(a), we analyze the behavior of the GH shift against the angle θ ranging from 0 to $\pi/2$ radians in the presence of non-zero α and β . We consider specific parameter values: $d_1 = 0.2\mu\text{m}$, $d_2 = 7.2\mu\text{m}$, $\epsilon_1 = 2.22$, $\epsilon_0 = 1$, $\epsilon_2 = 1 + \chi$, while keeping the remaining parameters consistent

with those presented in Fig. 2. Our investigation is primarily focused on understanding the GH shift's characteristics within regions characterized by normal dispersion in the intracavity CTL atomic medium, with the probe field detuning Δ_p set to $\Delta_p = 0.001\Gamma$ near the resonance. To simplify our analysis, we initially assume that the incident probe light beam is a plane wave. Notably, the results indicate positive GH shifts in the reflected probe light beams. This phenomenon can be attributed to the fact that, for reflected light, the cavity can experience a positive group index [refer to Fig. 3(a)], which can be approximated using the relation $N_g \approx (1/L)d\phi_r/d\omega_p$ [30].

2. Case 2: When α is nonzero and β zero

In Fig. 3(b), we once more chart the GH shift versus the incident angle θ . This time, we examine the intracavity atomic configuration in a manner where β is set to zero, while α remains nonzero, leading to an N -type configuration. The intracavity medium exhibits absorption with anomalous dispersion, resulting in a negative group index [see Fig. 2(b)]. As a consequence of this configuration, we observe a negative GH shift in relation to the angle θ [as depicted in Fig. 3(b)]. This negative shift arises due to the overall group index of the medium becoming negative.

3. Case 3: When α is zero and β nonzero

In Fig. 3(c), we present the GH shift plotted against the incident angle θ when β is nonzero while α is set to zero. In this specific case, the CTL model reduces to a Λ scheme, which is decoupled from the two-level system involving the states $|B_e\rangle$ and $|e\rangle$. In this case, as expected, the intracavity medium exhibits EIT with normal dispersion, resulting in a positive group index [see Fig. 2(c)]. Consequently, we observe a positive GH shift for all angles θ [as illustrated in Fig. 3(c)]. This positive shift is attributed to the overall group index of the medium becoming positive.

One can observe from the comparison between Figs. 3(a) and 3(c) that the GH shifts for the CTL model are nearly twice as large and more pronounced compared to those for the Λ model. This suggests the superiority of CTL over Λ in achieving substantial GH shifts.

It is essential to note that the analysis is based on the assumption that the incident light is a plane wave. The results and analysis are derived from the stationary-phase theory. Additionally, it is worth mentioning that the findings in Figs. 3(b) and 3(c) align with previously reported schemes involving four and three-level systems, which exhibit negative and positive GH shifts.

B. GH shift for incident Gaussian probe light beam

In this section, we examine a weak Gaussian probe light beam with a finite beam half width ω_s as it is incident on a three-layer medium featuring an intracavity medium consisting of a CTL atomic medium configuration. The electric field of this beam is expressed as follows [30,32]:

$$E_y^i(x, z) = \frac{1}{\sqrt{2\pi}} \int A(k_z) e^{i(k_x x + k_z z)} dk_z. \quad (17)$$

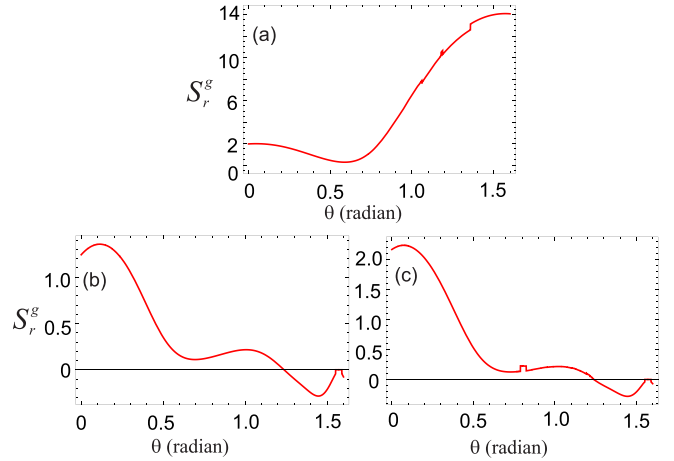


FIG. 4. The magnitude of GH shift (S_r^g) for Gaussian light beam versus angle of incidence (θ): (a) $\Omega_1 = 0.8\Gamma$, $\Omega_2 = 2\Gamma$, $\Omega_3 = 0.7\Gamma$, $\Omega_4 = \Gamma$, and $\phi = 0$ satisfying $\alpha \neq 0$ and $\beta \neq 0$; (b) $\Omega_1 = 0.7\Gamma$, $\Omega_2 = 0.7\Gamma$, $\Omega_3 = 0.8\Gamma$, $\Omega_4 = 0.8\Gamma$, and $\phi = 0$ satisfying $\beta = 0$ and $\alpha \neq 0$; (c) $\Omega_1 = 0.7\Gamma$, $\Omega_2 = 0.7\Gamma$, $\Omega_3 = 0.8\Gamma$, $\Omega_4 = 0.8\Gamma$, and $\phi = \pi$ fulfilling $\alpha = 0$ but $\beta \neq 0$. The other parameters are $d_1 = 0.2 \mu\text{m}$, $d_2 = 8 \mu\text{m}$, $\epsilon_1 = 2.22$, and $\epsilon_0 = 1$, $\omega_s = \lambda_p$, $\Delta_p = 0.5\Gamma$ and $\Gamma_e = \Gamma_b = \Gamma$.

Here, $A(k_z)$ represents the angular spectrum centered at $z = 0$ on the plane of $x = 0$ and is given by

$$A(k_z) = \frac{w_z}{\sqrt{2}} e^{-w_z^2(k_z - k_{z0})^2/4}, \quad (18)$$

where $w_z = \omega_s \sec(\theta)$, and $k_{z0} = k \sin(\theta)$, with θ and ω_s denoting the angle of incidence and the half beam width, respectively. Here, z corresponds to the distance from the center axis of the beam, with the Gaussian beam positioned at $z = 0$. Now, the reflected probe light beam from the proposed cavity can be written as [30,32]

$$E_y^r(x, z)|_{x<0} = \frac{1}{\sqrt{2\pi}} \int r(k_z, \omega_p) A(k_z) e^{-i(k_x x - k_z z)} dk_z.$$

The final expression of the Gaussian GH shift in the reflected beam S_r^g can be expressed as [30,32]

$$S_r^g = \frac{\int z |E_y^r(x, z)|^2 dz}{\int |E_y^r(x, z)|^2 dz}. \quad (19)$$

We employ the Gaussian incident light beam equations above to create a plot illustrating the GH shift concerning the reflected probe light beam at varying incident angles θ .

In Fig. 4, we compare the GH shift for Gaussian probe light with the incident angle θ across three different atomic configurations, mirroring the approach used for the plane wave in Fig. 3. For this plot, we take $w_s = \lambda_p$ for the beam half-width and set $\epsilon_1 = 2.22$, $\epsilon_0 = 1$, and $\epsilon_2 = 1 + \chi$. Figure 4 demonstrates the superior performance of the CTL model over the N and Λ schemes in generating larger positive GH shifts for the Gaussian beam. This is evident when comparing the magnitude of GH shifts for the CTL system [Fig. 4(a)] with those of the N [Fig. 4(b)] and Λ [Fig. 4(c)] schemes. It is noteworthy that the GH shifts for the CTL model remain entirely positive across the entire range of incident angles, whereas for the

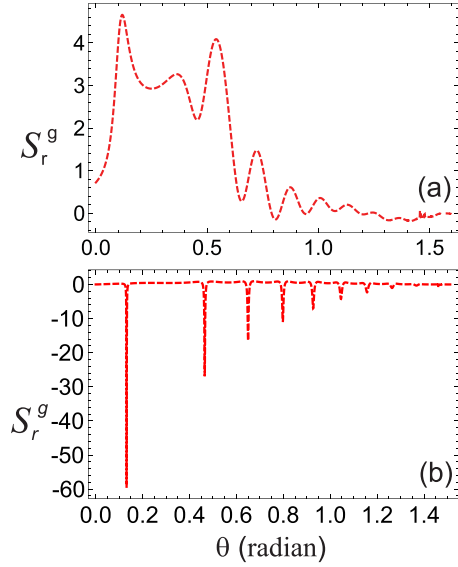


FIG. 5. The magnitude of GH shift (S_r^g) for Gaussian light beam versus angle of incidence (θ) for the case α and β are nonzero. (a) Beam half width $\omega_s = 2.5\lambda_p$, (b) $\omega_s = 25\lambda_p$. The other parameters are $\Omega_1 = 0.9\Gamma$, $\Omega_2 = 0.7\Gamma$, $\Omega_3 = 0.4\Gamma$, $\Omega_4 = 0.8\Gamma$, $\Delta_p = 0.001\Gamma$ and $\phi = 0$, $d_1 = 0.2\ \mu\text{m}$, $d_2 = 5\ \mu\text{m}$, $\epsilon_1 = 2.22$, and $\epsilon_0 = 1$.

N and Λ systems, the GH shifts become negative for angles ranging from 1.2 to $\pi/2$ radians. Through careful adjustment of system parameters, particularly the thickness values, the CTL model can achieve even more substantial GH shifts.

Next, we examine the impact of the beam width ω_s on our results, focusing on cases where both α and β exhibit nonzero values (CTL setup). In Fig. 5(a), we choose a smaller width, setting $\omega_s = 2.5\lambda_p$ for the incident light beam. Conversely, in Fig. 5(b), we consider a significantly larger ω_s for the incident light beam, specifically $\omega_s = 25\lambda_p$, in comparison to the wavelength of the incident probe light beam λ_p . We then investigate the GH shift across different incident angles, observing the effect of ω_s on the GH shifts. In Fig. 5(a) with $\omega_s = 2.5\lambda_p$, a positive GH shift is observed for the majority of incident angles. However, in Fig. 5(b) with $\omega_s = 25\lambda_p$, the GH shift transitions to negative values at specific angles. This suggests that for smaller beam widths, the GH shift consistently maintains a positive value across the incident angles, while it diminishes or undergoes a transformation from positive to negative for larger ω_s values.

To gain a clearer understanding and further illustrate the dependence of GH shifts on small or large beam width ω_s , as observed in Fig. 5, we present in Fig. 6 the GH shifts plotted against the beam width for two distinct values of θ : $\theta = 0.13$ radians [Fig. 6(a)] and $\theta = 0.55$ radians [Fig. 6(b)]. In Fig. 6(a), with $\theta = 0.13$ radians, we observe that the GH shift of reflected Gaussian beam is positive for smaller beam widths, approximately up to $5\lambda_p$. Beyond this threshold, the GH shift becomes negative, reaching a maximum negative value. Nevertheless, with a further increase in the beam width, it approaches zero. In Fig. 6(b), where $\theta = 0.55$ radians, we observe a consistently positive GH shift as the beam width varies from 0 to $80\lambda_p$. For smaller beam widths, the GH shift initially increases with a slight increment in ω_s . How-

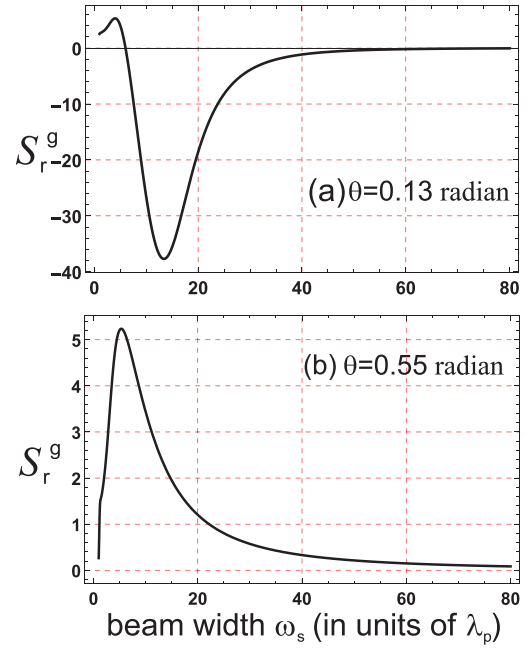


FIG. 6. The magnitude of GH shift (S_r^g) for Gaussian light beam versus beam half width ω_s for α and β are nonzero. The other parameters are $\Omega_1 = 0.9\Gamma$, $\Omega_2 = 0.7\Gamma$, $\Omega_3 = 0.4\Gamma$, $\Omega_4 = 0.8\Gamma$, $\Delta_p = 0.001\Gamma$, $\phi = 0$, $d_1 = 0.2\ \mu\text{m}$, $d_2 = 5\ \mu\text{m}$, $\epsilon_1 = 2.22$, and $\epsilon_0 = 1$.

ever, as ω_s continues to increase, the GH shift begins to decrease, eventually approaching zero at $\omega_s = 80\lambda_p$. These results closely correspond to those depicted in Fig. 5, wherein at $\theta = 0.13$ radians, the GH shift was positive for a smaller width of $\omega_s = 2.5\lambda_p$ [Fig. 5(a)], while it changed to negative for a larger width of $\omega_s = 25\lambda_p$ [Fig. 5(b)]. However, at $\theta = 0.55$ radians, the GH shift was positive for a smaller width of $\omega_s = 2.5\lambda_p$ [Fig. 5(a)], whereas it diminished to become negligible for a larger width of $\omega_s = 25\lambda_p$ [Fig. 5(b)].

V. EFFECT OF DOPPLER BROADENING

Thus far, the GH shift has been studied primarily in a cold atomic system, with the assumption that atoms are motionless. For an experimentally viable system, it is essential to consider schemes that operate at room temperature, where the motion of atoms within the atomic medium becomes a significant factor. As temperature increases, atoms gain kinetic energy and move faster. This motion causes Doppler broadening (DB) in both the absorptive and dispersive spectra of the atomic medium. Changes in temperature and DB can alter the characteristics of the intracavity medium [52]. Consequently, it is important to investigate the behavior of the GH shift in a thermally active medium and understand the implications of introducing DB into the model. To explore the impact of DB on GH shifts, we focus specifically on the case of CTL atoms.

When light interacts with atoms undergoing thermal motion, a slight frequency variation occurs due to the Doppler effect induced by the atoms' movement relative to the light pulse. The average velocities of these moving atoms within the intracavity medium can be determined using the Maxwell Boltzmann velocity distribution function, indicating that the

atoms adhere to this distribution [53,54]. The interplay between the atoms' motion and the optical field alters the medium's response, wherein the optical detuning is replaced by $\Delta_p + k_p v$ in the susceptibility equation χ [as expressed in Eqs. (9) and (10)]. Consequently, the modified optical susceptibility χ^{DB} takes the form

$$\chi^{\text{DB}} = \eta \langle \rho_{ba} \rangle_v, \quad (20)$$

$$\langle \rho_{ba} \rangle_v = \frac{1}{\sqrt{2\pi D}} \int \rho_{ba}(\Delta_p + k_p v) e^{-\frac{v^2}{2D^2}} dv, \quad (21)$$

where D represents the Doppler effect accounting for the ensemble of atoms in thermal motion, which can be determined by utilizing

$$D = \sqrt{\frac{2k^2 k_b T}{M}}. \quad (22)$$

Here, M represents the mass of the atom, k_b denotes the Boltzmann constant, and T stands for the absolute temperature. To analyze GH-shift behavior, we examine the reflection of an incident electromagnetic wave within the cavity, potentially resulting in a shift in the reflected portion. The intracavity medium's permittivity is then modified by the DB effect, described by the relation $\epsilon_2 = 1 + \chi^{\text{DB}}$.

The GH shift in the reflected beam for plane probe light can be determined using the equations provided in Eq. (16). Let us consider an incident light beam originating from the vacuum, where $\epsilon_0 = 1$, onto a cavity composed of three layers. Within this setup, a CTL scheme with an EIT configuration is positioned between two dielectric slabs, forming an angle θ with respect to the normal axis, as illustrated in Fig. 1.

In Figs. 7(a) and 7(b), we investigate the behavior of the GH shift for incident angles θ in the presence of DB with a plane wave and a Gaussian probe light beam, respectively, for a Doppler width of $D = 100$ MHz, which is relevant to the room temperature Doppler width of Rb 87. Except for some specific angles in the case of the plane wave for which the GH shift becomes negative, a positive trend in GH shifts for various incident angles is observed. The maximum shift amplitude is slightly reduced now when considering the effect of DB compared to the cold CTL model when DB is not considered.

VI. EXPERIMENTAL REALIZATION OF THE PROPOSED MODEL

The detailed schematic of the CTL system is illustrated in Fig. 8(a). For ^{87}Rb atoms, the proposed implementation involves a combined tripod and Λ configuration. The CTL system includes two excited states, $|b\rangle = |5P_{3/2}, F = 1, m_F = 0\rangle$, and $|e\rangle = |5P_{3/2}, F = 0, m_F = 0\rangle$, as well as three lower states, $|a\rangle = |5S_{1/2}, F = 2, m_F = 1\rangle$, $|c\rangle = |5S_{1/2}, F = 1, m_F = 1\rangle$, and $|d\rangle = |5S_{1/2}, F = 1, m_F = -1\rangle$. It is important to note that a second probe beam cannot be generated due to the forbidden transition from $|a\rangle$ to $|e\rangle$. The polarization configuration in this implementation is as follows: Ω_p is either σ_+ or σ_- , Ω_1 and Ω_3 are σ_+ , and Ω_2 and Ω_4 are σ_- , as shown in Fig. 8(b). In this way the ground state driven by Ω_p is isolated from the control fields $\Omega_1, \Omega_2, \Omega_3$, and Ω_4 , as they drive different hyperfine levels.

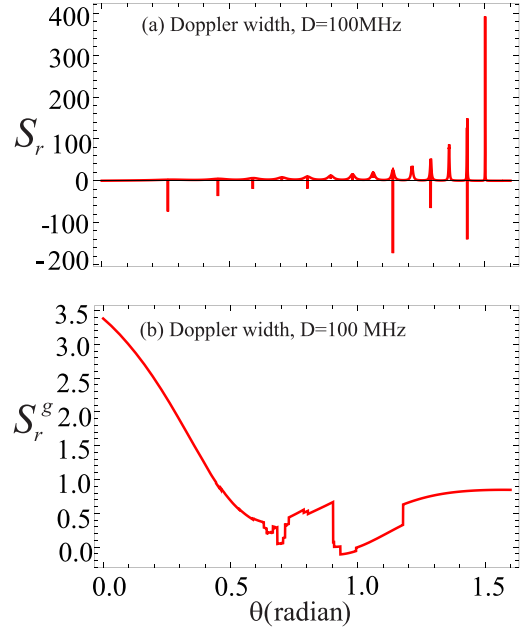


FIG. 7. (a) The magnitude of GH shift (S_r) for plane probe beam versus angle of incidence (θ) for CTL scheme for Doppler width $D = 100$ MHz. (b) The magnitude of GH shift (S_r) for Gaussian probe light beam versus angle of incidence (θ) for CTL scheme for Doppler width $D = 100$ MHz. The other parameters consider are $\Omega_1 = 1.5\Gamma$, $\Omega_2 = 3\Gamma$, $\Omega_3 = 2.5\Gamma$, $\Omega_4 = 0.9\Gamma$, and $\phi = 0$ satisfying $\alpha \neq 0$ and $\beta \neq 0$, $d_1 = 0.2 \mu\text{m}$, $d_2 = 7.2 \mu\text{m}$, $\epsilon_1 = 2.22$, $\epsilon_0 = 1$, $\Delta_p = 0.001\Gamma$, and $\Gamma_e = \Gamma_b = \Gamma$.

Assuming that initially only state $|a\rangle$ is populated prevents the field Ω_2 (Ω_1) from exciting the $m_F = 0 \rightarrow m_F = +1$ ($m_F = 0 \rightarrow m_F = -1$) transition, as these states do not participate in the overall scheme. Consequently, the transition from $m_F = 0 \rightarrow m_F = +1$ ($m_F = 0 \rightarrow m_F = -1$) induced by Ω_2 (Ω_1) would occur between unoccupied levels. Populating only the state $|5S_{1/2}, F = 2, m_F = 1\rangle$ initially (e.g., by optically pumping atoms to this state) also avoids a TE polarization probe field to couple various magnetic sublevels of $|5S_{1/2}, F = 2\rangle$ and $|5P_{3/2}, F = 1\rangle$. A detailed description of a possible experiment is beyond the scope of this article.

In our simulations, we use a detuning of $\Delta_p = 0.001\Gamma$ to analyze the GH shifts very close to resonance. This small detuning was chosen deliberately to clearly illustrate the theoretical behavior in an idealized condition and to highlight the advantages of the CTL lower Λ and N schemes, particularly due to the EIT and dispersive properties of CTL near resonance. Given that Γ is on the order of MHz, the chosen detuning of Δ_p corresponds to a value on the order of kHz. For practical implementations, where achieving such a small detuning might be challenging due to phase noise limitations with typical light sources, using larger detuning values could be more feasible to mitigate phase noise issues. However, this would require careful adjustment of other system parameters, including Rabi frequencies and thickness values, to optimize the experimental results.

In our theoretical model, Eqs. (8) assume a weak probe field Ω_p , allowing us to linearize the density matrix equations and consider only the first-order terms in Ω_p . Under this

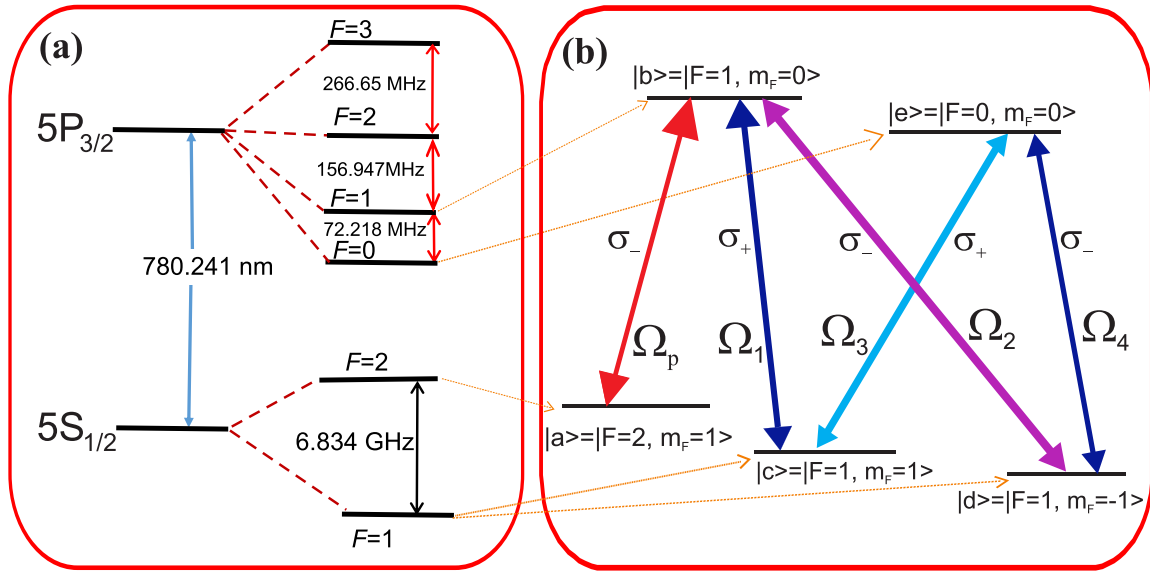


FIG. 8. (a) Hyperfine-level structure diagram of CTL type ^{87}Rb five-level atomic system. (b) Schematic of five-level combined tripod and Λ atomic system. Transitions are controlled by the probe and control fields. The Ω_p , Ω_1 , Ω_2 , Ω_3 , and Ω_4 shows the Rabi frequencies.

approximation, the total decay rates Γ_b and Γ_e are relevant, representing the sum of the branching ratios from the excited states to all lower states. This simplifies our analysis by focusing on the primary effects of Doppler broadening and probe beam characteristics on the GH shifts, without considering specific decay pathways. While $\Gamma_b = \Gamma_e = \Gamma$ is assumed for the $5P_{3/2}$ state of Rb 87, including individual branching ratios would provide a more detailed description. Note that the Rabi frequencies depend on the Clebsch-Gordan coefficients, so the laser intensities should be chosen accordingly.

VII. CONCLUDING REMARKS

In conclusion, we studied the interaction of a five-level CTL atomic medium housed within a cavity, subjected to four strong laser fields making a closed-loop structure. By manipulating the light fields, this system can effectively transition between a Λ -shaped or N -shaped configuration. Our investigation primarily focused on the dynamic alterations of the GH shift in reflection for both incident plane and Gaussian probe light beams. Throughout our investigation, we showcased the clear advantage of the CTL configuration over both Λ and N schemes in achieving significant positive GH shifts, regardless of whether the incident light was in the form of a plane or Gaussian beam. Notably, we found a crucial influence exerted by the beam width on the control of GH-shift magnitude and sign, a factor that emerged prominently when analyzing Gaussian probe light. Our proposed tunable GH-shift model in the CTL system holds promise for various applications, particularly in sensor devices and optical switches. This research opens up new avenues for harnessing the GH shift as a versatile tool in optical manipulation and control, with

potential implications for advancing technology and scientific understanding.

It should be noted that the dark or bright states in EIT can form after multiple cycles, but the final steady state [as described in Eq. (9)] will remain the same [55–57]. While dynamic processes occur at intermediate times [58–60], our analysis focuses on the system once it reaches a steady state. It is important to recognize that if the system is not entirely closed (e.g., Ref. [58]), there could be population leakage, which would result in not all atoms being involved in the EIT formation. This issue can be mitigated by adequately preparing the atomic population. Alternatively, as shown in Ref. [27], using appropriate laser detuning can help prevent such leakage.

ACKNOWLEDGMENTS

H.R.H. gratefully acknowledges Prof. Ite A. Yu for his valuable discussions on the CTL scheme implementation. S.H.A. acknowledges valuable discussions with Prof. Reza Asgari. P.Z. acknowledges support by the National Nature Science Foundation of China (Grant No. 12174301), the Natural Science Basic Research Program of Shaanxi (Grant No. 2023-JC-JQ-01), and the Open Fund of State Key Laboratory of Acoustics (Grant No. SKLA202312).

M.A. performed check-in numerical simulations generated all numerical results presented in the paper and drafted the initial version. S.H.A., Z., P.Z., and J.R. contributed to reviewing and editing and conducted a formal analysis of the results. H.R.H. conceived the idea and guided the research. All the authors contributed to the discussion of the results and the manuscript preparation and revision.

[1] B. M. Jost, A.-A. R. Al-Rashed, and B. E. A. Saleh, Observation of the Goos-Hänchen effect in a phase-conjugate mirror, *Phys. Rev. Lett.* **81**, 2233 (1998).

[2] C. W. J. Beenakker, R. A. Sepkhanov, A. R. Akhmerov, and J. Tworzydło, Quantum Goos-Hänchen effect in graphene, *Phys. Rev. Lett.* **102**, 146804 (2009).

- [3] V.-O. de Haan, J. Plomp, T. M. Rekveldt, W. H. Kraan, and van A. A. Well, Observation of the Goos-Hänchen shift with neutrons, *Phys. Rev. Lett.* **104**, 010401 (2010).
- [4] Y. Fan, N. H. Shen, F. Zhang, Z. Wei, H. Li, Q. Zhao, Q. Fu, P. Zhang, T. Koschny, and C. M. Soukoulis, Electrically tunable Goos-Hänchen effect with graphene in the terahertz regime, *Adv. Opt. Mater.* **4**, 1824 (2016).
- [5] T. Shui, W.-X. Yang, Q. Zhang, X. Liu, and L. Li, Squeezing-induced giant Goos-Hänchen shift and hypersensitized displacement sensor in a two-level atomic system, *Phys. Rev. A* **99**, 013806 (2019).
- [6] Q. You, Y. Shan, S. Gan, Y. Zhao, X. Dai, and Y. Xiang, Giant and controllable Goos-Hänchen shifts based on surface plasmon resonance with graphene-MoS₂ heterostructure, *Opt. Mater. Express* **8**, 3036 (2018).
- [7] V. K. Ignatovich, Neutron reflection from condensed matter, the Goos-Hänchen effect and coherence, *Phys. Lett. A* **322**, 36 (2004).
- [8] R. Briers, O. Leroy, and G. Shkerdin, Bounded beam interaction with thin inclusions. Characterization by phase differences at Rayleigh angle incidence, *J. Acoust. Soc. Am.* **108**, 1622 (2000).
- [9] X. Zeng, M. Al-Amri, and M. S. Zubairy, Tunable Goos-Hänchen shift from graphene ribbon array, *Opt. Express* **25**, 23579 (2017).
- [10] R. U. Din, X. Zeng, I. Ahmad, and G.-Q. Ge, Enhanced and highly tunable Goos-Hänchen shifts at a nanocomposite-graphene interface, *Appl. Phys. Lett.* **114**, 161902 (2019).
- [11] I. V. Soboleva, V. V. Moskalenko, and A. A. Fedyanin, Giant Goos-Hänchen effect and Fano resonance at photonic crystal surfaces, *Phys. Rev. Lett.* **108**, 123901 (2012).
- [12] P. T. Leung, C. W. Chen, and H.-P. Chiang, Large negative Goos-Hänchen shift at metal surfaces, *Opt. Commun.* **276**, 206 (2007).
- [13] M. Merano, A. Aiello, G. W'tHooft, M. P. van Exter, E. R. Eliel, and J. P. Woerdman, Observation of Goos-Hänchen shifts in metallic reflection, *Opt. Express* **15**, 15928 (2007).
- [14] J. Fan, A. Dogariu, and L. J. Wang, Amplified total internal reflection, *Opt. Express* **11**, 299 (2003).
- [15] F. Goos and H. Hänchen, Ein neuer und fundamentaler versuch zur totalreflexion, *Ann. Phys. (Leipzig)* **436**, 333 (1947).
- [16] K. Artmann, Berechnung der seitenversetzung des totalreflektierten strahles, *Ann. Phys. (Leipzig)* **437**, 87 (1948).
- [17] F. Goos and H. Hänchen, Neumessung des strahlwersetzungseffektes bei totalreflexion, *Ann. Phys. (Leipzig)* **440**, 251 (1949).
- [18] R. H. Renard, Total reflection: A new evaluation of the Goos-Hänchen shift, *J. Opt. Soc. Am.* **54**, 1190 (1964).
- [19] E. Pfleghaar, A. Marseille, and A. Weis, Quantitative investigation of the effect of resonant absorbers on the Goos-Hnchen shift, *Phys. Rev. Lett.* **70**, 2281 (1993).
- [20] R. Kondo, S. Tojo, T. Fujimoto, and M. Hasuo, Shift and broadening in attenuated total reflection spectra of the hyperfine-structure-resolved D_2 line of dense rubidium vapor, *Phys. Rev. A* **73**, 062504 (2006).
- [21] Y. Wan, Z. Zheng, and J. Zhu, Experimental observation of the propagation-dependent beam profile distortion and Goos-Hänchen shift under the surface plasmon resonance condition, *J. Opt. Soc. Am. B* **28**, 314 (2011).
- [22] Y. Wan, Z. Zheng, W. Kong, X. Zhao, and J. Liu, Fiber-to-fiber optical switching based on gigantic Bloch-surface-wave-induced Goos-Hänchen shifts, *IEEE Photon. J.* **5**, 7200107 (2013).
- [23] C. Xu, J. Xu, G. Song, C. Zhu, Y. Yang, and G. S. Agarwal, Enhanced displacements in reflected beams at hyperbolic metamaterials, *Opt. Express* **24**, 21767 (2016).
- [24] T. Yu, H. Li, Z. Cao, Y. Wang, Q. Shen, and Y. He, Oscillating wave displacement sensor using the enhanced Goos-Hänchen effect in a symmetrical metal-cladding optical waveguide, *Opt. Lett.* **33**, 1001 (2008).
- [25] M. Tang, M. Ran, F. Chen, X. Wang, H. Li, X. Chen, and Z. Cao, Narrow band optical filter using Goos-Hänchen shift in a cascaded waveguide structure, *Opt. Laser Technol.* **55**, 42 (2014).
- [26] L. G. Wang and S. Y. Zhu, Large positive and negative Goos-Hänchen shifts from a weakly absorbing left-handed slab, *J. Appl. Phys.* **98**, 043522 (2005).
- [27] L. G. Wang, M. Ikram, and M. S. Zubairy, Control of the Goos-Hänchen shift of a light beam via a coherent driving field, *Phys. Rev. A* **77**, 023811 (2008).
- [28] Ziauddin, S. Qamar and M. S. Zubairy, Coherent control of the Goos-Hänchen shift, *Phys. Rev. A* **81**, 023821 (2010).
- [29] Ziauddin and S. Qamar, Gain-assisted control of the Goos-Hänchen shift, *Phys. Rev. A* **84**, 053844 (2011).
- [30] Ziauddin and S. Qamar, Control of the Goos-Hänchen shift using a duplicated two-level atomic medium, *Phys. Rev. A* **85**, 055804 (2012).
- [31] L. G. Wang, S. Y. Zhu, and M. S. Zubairy, Goos-Hänchen shifts of partially coherent light fields, *Phys. Rev. Lett.* **111**, 223901 (2013).
- [32] M. Abbas, Ziauddin and S. Qamar, Amplitude control of the Goos-Hänchen shift via a Kerr nonlinearity, *Laser Phys. Lett.* **11**, 015201 (2014).
- [33] H. R. Hamed, A. Radmehr, and M. Sahrai, Manipulation of Goos-Hänchen shifts in the atomic configuration of mercury via interacting dark-state resonances, *Phys. Rev. A* **90**, 053836 (2014).
- [34] S. Asiri, J. Xu, M. A. Amri, and M. S. Zubairy, Controlling the Goos-Hänchen and Imbert-Fedorov shifts via pump and driving fields, *Phys. Rev. A* **93**, 013821 (2016).
- [35] Z. Uddin and S. Qamar, Effect of width of incident Gaussian beam on the longitudinal shifts and distortion in the reflected beam, *Opt. Commun.* **319**, 1 (2017).
- [36] M. Abbas, Ziauddin, and S. Qamar, Goos-Hänchen shift of partially coherent light fields in double quantum dots, *J. Opt. Soc. Am. B* **34**, 245 (2017).
- [37] Ghaisuddin, Ziauddin, M. Abbas, and L.-G. Wang, Magnitude of the Goos-Hänchen shift depends on the beam propagation in a medium, *J. Opt. Soc. Am. B* **36**, 119 (2019).
- [38] K. V. Sreekanth, Q. Ouyang, S. Han, K.-T. Yong, and R. Singh, Giant enhancement in Goos-Hänchen shift at the singular phase of a nanophotonic cavity, *Appl. Phys. Lett.* **112**, 161109 (2018).
- [39] X. Yin and L. Hesselink, Goos-Hänchen shift surface plasmon resonance sensor, *Appl. Phys. Lett.* **89**, 261108 (2006).
- [40] G. Sui, L. Cheng, and L. Chen, Large positive and negative lateral optical beam shift due to long-range surface plasmon resonance, *Opt. Commun.* **284**, 1553 (2011).

- [41] L. Chen, X. Liu, Z. Cao, and S. Zhuang, Mechanism of giant Goos-Hänchen effect enhanced by long-range surface plasmon excitation, *J. Opt.* **13**, 035002 (2011).
- [42] V. J. Yallapragada, A. P. Ravishankar, G. L. Mulay, G. S. Agarwal, and V. G. Achanta, Observation of giant Goos-Hänchen and angular shifts at designed metasurfaces, *Sci. Rep.* **6**, 19319 (2016).
- [43] H. Mao, T. Zang, J. Sun, T. Pan, and G. Xu, Nonlinear Goos-Hänchen shifts of reflected light from inhomogeneous Kerr-like slabs, *Phys. Lett. A* **377**, 1503 (2013).
- [44] J.-H. Kang, S. Wang, Z. Shi, W. Zhao, E. Yablonovitch, and F. Wang, Goos-Hänchen shift and even-odd peak oscillations in edge reflections of surface polaritons in atomically thin crystals, *Nano Lett.* **17**, 1768 (2017).
- [45] R.-F. Zheng, L. Zhou, and W. Zhang, A beam splitter for Dirac-Weyl fermions through the Goos-Hänchen-like shift, *Phys. Lett. A* **381**, 3798 (2017).
- [46] A. Farmani, M. Miri, and M. H. Sheikhi, Tunable resonant Goos-Hänchen and Imbert Fedorov shifts in total reflection of terahertz beams from graphene plasmonic metasurfaces, *J. Opt. Soc. Am. B* **34**, 1097 (2017).
- [47] Y. Hirai, K. Matsunaga, Y. Neo, T. Matsumoto, and M. Tomita, Observation of Goos-Hänchen shift in plasmon-induced transparency, *Appl. Phys. Lett.* **112**, 051101 (2018).
- [48] Y. Cao, Y. Fu, Q. Zhou, Y. Xu, L. Gao, and H. Chen, Giant Goos-Hänchen shift induced by bounded states in optical PT -symmetric bilayer structures, *Opt. Express* **27**, 7857 (2019).
- [49] S. Khan, F. Shafiq, and S. A. Ullah, Giant lateral shift via atom cavity coupling, *J. Opt. Soc. Am. B* **36**, 383 (2019).
- [50] H. R. Hamed, J. Ruseckas, and G. Juzeliūnas, Electromagnetically induced transparency and nonlinear pulse propagation in a combined tripod and Λ atom-light coupling scheme, *J. Phys. B: At. Mol. Opt. Phys* **50**, 185401 (2017).
- [51] H. R. Hamed, V. Kudriašov, J. Ruseckas, and G. Juzeliūnas, Azimuthal modulation of electromagnetically induced transparency using structured light, *Optics Express* **26**, 28249 (2018).
- [52] L. Zhang, F. Zhou, Y. Niu, J. Zhang, and S. Gong, The effect of Doppler broadening on dispersive and absorptive properties in atomic systems with two-photon interference, *Opt. Commun.* **284**, 5697 (2011).
- [53] E. Fermi, Quantum theory of radiations, *Rev. Mod. Phys.* **4**, 87 (1932).
- [54] G. S. Agarwal and T. N. Dey, Slow light in Doppler-broadened two-level systems, *Phys. Rev. A* **68**, 063816 (2003).
- [55] E. Paspalakis and P. L. Knight, Electromagnetically induced transparency and controlled group velocity in a multilevel system, *Phys. Rev. A* **66**, 015802 (2002).
- [56] M. Fleischhauer, A. Imamoglu, and J. P. Marangos, Electromagnetically induced transparency: Optics in coherent media, *Rev. Mod. Phys.* **77**, 633 (2005).
- [57] R. Finkelstein, S. Bali, O. Firstenberg, and I. Novikova, A practical guide to electromagnetically induced transparency in atomic vapor, *New J. Phys.* **25**, 035001 (2023).
- [58] I. V. Jyotsna and G. S. Agarwal, Coherent population trapping at low light levels, *Phys. Rev. A* **52**, 3147 (1995).
- [59] H. Y. Ling, Y.-Q. Li, and M. Xiao, Coherent population trapping and electromagnetically induced transparency in multi-Zeeman-sublevel atoms, *Phys. Rev. A* **53**, 1014 (1996).
- [60] J. Choi and D. S. Elliott, Influence of interaction time and population redistribution on the localization of atomic excitation through electromagnetically induced transparency, *Phys. Rev. A* **89**, 013414 (2014).